Electronic Supplementary Information

Reduction of hexaazatrinaphthylenes by divalent lanthanocenes leads to ligand-based multiconfigurational properties

Siobhan R. Temple,[a] Jinkui Tang,[b] Graham J. Tizzard,[c] Akseli Mansikkamäki,*[d] Richard A. Layfield*[a]

[a] Department of Chemistry, School of Life Sciences, University of Sussex, Brighton, BN1 9QR, UK.
[b] Changchun Institute of Applied Chemistry, Chinese Academy of Sciences, Renmin Street 5626, 130022 Changchun, China.
[c] School of Chemistry, University of Southampton, University Road, Southampton, SO17 1BJ, UK.
[d] NMR Research Unit, University of Oulu, P. O. Box 8000, FI-90014, Finland.
E-mail: R.Layfield@sussex.ac.uk, Akseli.Mansikkamaki@oulu.fi

Contents

General considerations

All manipulations were performed under anaerobic and anhydrous conditions using Schlenk line or glovebox techniques, unless otherwise stated. Benzene and toluene were refluxed for a minimum of three days over molten potassium, degassed by freeze-pump-thaw cycles, and stored over a potassium mirror or activated 4 Å molecular sieves. NMR spectra were recorded on a Varian VNMR S400 spectrometer. Elemental analyses were carried at Elemental Lab (Okehampton, UK) or Mikroanalaytisches Labor Pascher (Remagen, Germany). UV/vis/NIR spectra were recorded using J-Young adapted quartz cuvettes on a Shimadzu UV-3600 Plus spectrometer, and FTIR spectra were recorded on a Bruker Alpha spectrometer with platinum-diamond ATR module housed within a glovebox. Literature procedures were used to synthesize [Cp*$_2$Yb(OEt$_2$)], [Cp*$_2$Sm(THF)$_2$], hexaazaatrinaphthylene (HAN) and hexamethylhexaazaatrinaphthylene (Me$_6$HAN).[1–3]

Synthesis of [(Cp*$_2$Sm)$_3$HAN]·C$_7$H$_8$ (**1$_{Sm}$**·C$_7$H$_8$)

Solid HAN (23.0 mg, 0.06 mmol) was added to a solution of [Cp*$_2$Sm(THF)$_2$] (101.0 mg, 0.18 mmol) in toluene (15 mL) and the resulting dark red solution was left stirring at room temperature for 30 minutes. The reaction mixture was filtered, concentrated, and stored at –40 °C for three days. Brown crystals of **1$_{Sm}$**·C$_7$H$_8$ were isolated and dried under reduced pressure (59.0 mg, 57%). ^{1}H NMR (400 MHz, D$_8$-tol, δ/ppm): –64.63(s, 6H, HAN-CH), –37.75 (s, 6H, HAN-CH), 2.91 (s, 90H, Cp*). FTIR ($\bar{\nu}$/cm^{-1}): 3033, 2884, 2845, 2430, 1865, 1787, 1557, 1457, 1411, 1356, 1309, 1248, 1199, 1149, 1131, 1075, 1022, 892, 781, 727, 669, 613, 493. Elemental analysis (%), found (calculated) for **1$_{Sm}$**·C$_7$H$_8$: C 62.75 (62.85), H 5.96 (6.38), N 5.11 (4.83).

Synthesis of $[(C_5Me_5)_2Yb)_3HAN]\cdot C_7H_8$ ($\mathbf{1}_{Yb}\cdot C_7H_8$)

Compound $\mathbf{1}_{Yb}$ was synthesised using the procedure described for $\mathbf{1}_{Sm}$, using $[Cp^*_2Yb(OEt_2)]$ (75.0 mg, 0.145 mmol) and HAN (18.5 mg, 0.048 mmol). Storage of a concentrated toluene solution at –40 °C for three days resulted in the formation of red crystals of $\mathbf{1}_{Yb}\cdot C_7H_8$ (55.0 mg, 63 %).^{1}H NMR (400 MHz, D_8-tol, δ/ppm): –2.57 (s, 90H, Cp*), 0.37 (s, 6H, HAN-CH), 93.38 (s, 6H, HAN-CH). FTIR ($\bar{\nu}$/cm^{-1}): 3034, 2971, 2900, 2845, 1554, 1463, 1418, 1372,1317, 1246, 1205, 1144, 1128, 1073, 1019, 893, 784, 736, 713, 627, 588, 485. Elemental analysis (%), found (calculated) for $\mathbf{1}_{Yb}\cdot C_7H_8$: C 60.39 (60.48), H 6.01 (6.14), N 4.78 (4.65).

Synthesis of $[(C_5Me_5)_2Sm)_3HANMe_6]\cdot 2.5(C_6H_6)$ ($\mathbf{2}_{Sm}\cdot 2.5(C_6H_6)$)

Solid Me_6HAN (46.4 mg, 0.10 mmol) was added to a solution of $[Cp^*_2Sm(THF)_2]$ (168.0 mg, 0.30 mmol) in benzene (5 mL). The reaction mixture was briefly swirled and left to stand overnight at room temperature, which resulted in the formation of red crystals of $\mathbf{2}_{Sm}\cdot 2.5(C_6H_6)$ suitable for X-ray diffraction. The red crystals were subsequently isolated by filtration and dried under reduced pressure. The ^{1}H NMR spectrum revealed partial removal of the lattice solvent to give $\mathbf{2}_{Sm}\cdot 0.5(C_6H_6)$ as red polycrystalline material (123.0 mg, 69 %). ^{1}H NMR (400 MHz, D_8-tol, δ/ppm): –61.08 (s, 6H, HAN CH), 3.00 (s, 90H, Cp*), 33.50 (s, 18H, HAN CH_3). FTIR ($\bar{\nu}$/cm^{-1}): 3036, 2964, 2891, 2847, 1539, 1404, 1314, 1259, 1204, 1099, 1084, 1017, 1000, 831, 674, 635, 610, 472, 416. Elemental analysis (%) found (calculated) for $\mathbf{2}_{Sm}\cdot 0.5(C_6H_6)$: C 61.90 (63.10), H 6.51 (6.66), N 3.96 (4.75).

Synthesis of $[(C_5Me_5)_2Yb)_3HANMe_6]\cdot 2(C_6H_6)$ ($\mathbf{2}_{Yb}\cdot 2(C_6H_6)$)

Solid Me_6HAN (24.0 mg, 0.051 mmol) was added to a solution of $[Cp^*_2Yb(OEt_2)]$ (79.0 mg, 0.153 mmol) in benzene (5 mL). The reaction mixture was briefly swirled and left to stand overnight at room temperature, which resulted in the formation of red crystals of $\mathbf{2}_{Yb}\cdot 2(C_6H_6)$ suitable for X-ray diffraction. The red crystals were subsequently isolated by filtration and dried under reduced pressure. The ^{1}H NMR spectrum revealed partial removal of the lattice solvent to give $\mathbf{2}_{Yb}\cdot 0.5(C_6H_6)$ as red polycrystalline material (86 mg, 92%). ^{1}H NMR (400 MHz, D_8-tol, δ/ppm): 92.86 (s, 18H, HAN CH_3), –2.91 (s, 90H, Cp*) (the HAN aromatic CH protons were not observed). FTIR ($\bar{\nu}$/cm^{-1}): 3033, 2965, 2888, 2849, 1540, 1480, 1403, 1312, 1255, 1202, 1098, 1085, 1016, 999, 836, 671, 632, 469, 417. Elemental analysis (%) found (calculated) for $\mathbf{2}_{Yb}\cdot 0.5(C_6H_6)$: C 60.93 (60.77), H 6.35 (6.42), N 4.33 (4.57).

X-ray crystallography

Data for $\mathbf{1_{Sm}}\cdot C_7H_8$ were collected on a Rigaku FR-007HF rotating anode diffractometer using CuK$_\alpha$ radiation (λ = 1.54184 Å), equipped with Saturn 724+ CCD area detector and a quarter-chi goniometer performing ω scans to fill the Ewald sphere at 100 K. Measurements on $\mathbf{1_{Yb}}\cdot C_7H_8$ were made using an Agilent Gemini Ultra diffractometer using CuK$_\alpha$ radiation (λ = 1.54184 Å). Measurements on $\mathbf{2_{Sm}}\cdot 2.5(C_6H_6)$ and $\mathbf{2_{Yb}}\cdot 2(C_6H_6)$ were carried out at the EPSRC National Crystallography Service at the University of Southampton. For $\mathbf{2_{Yb}}\cdot 2(C_6H_6)$, measurements were collected on a Rigaku 007HF diffractometer equipped with Arc-Sec VHF Varimax confocal mirrors and a UG2 goniometer and HyPix Arc-100 detector performing ω scans to fill the Ewald sphere at 100 K. For $\mathbf{2_{Sm}}\cdot 2.5(C_6H_6)$, measurements were collected on a Rigaku FRE+ Rotating Anode (Mo-K$_\alpha$) source, equipped with a UG2 goniometer and HyPix 6000HE detector performing ω scans to fill the Ewald sphere at 100 K. Structures $\mathbf{1_{Sm}}\cdot C_7H_8$, $\mathbf{1_{Yb}}\cdot C_7H_8$ and $\mathbf{2_{Yb}}\cdot 2(C_6H_6)$ were solved with SHELXT using structural refinement and using least squares minimisation with SHELXL ($\mathbf{1_{Sm}}\cdot C_7H_8$, $\mathbf{1_{Yb}}\cdot C_7H_8$) or olex2.refine ($\mathbf{2_{Yb}}\cdot 2(C_6H_6)$) within Olex2. Isotropic and anisotropic thermal parameters were used for hydrogen atoms and non-hydrogen atoms respectively.[4–6] For $\mathbf{2_{Sm}}\cdot 3(C_6H_6)$, the data was solved using hklf4 with SHELXT and refined against hklf5 using olex2.refine. Weak high angle data and two components were found, which allowed the atom connectivity to be established.

Table S1. Crystal data and structure refinement details.

	$\mathbf{1_{Sm}}\cdot C_7H_8$	$\mathbf{1_{Yb}}\cdot C_7H_8$	$\mathbf{2_{Sm}}\cdot 2.5(C_6H_6)$	$\mathbf{2_{Yb}}\cdot 2(C_6H_6)$
Empirical formula	$C_{91}H_{110}N_6Sm_3$	$C_{91}H_{110}N_6Yb_3$	$C_{105}H_{129}N_6Sm_3$	$C_{102}H_{126}N_6Yb_3$
Formula weight	1738.89	1809.96	1926.334	1955.291
T/K	100.00(10)	100.0(3)	100(2)	100.00(10)
Crystal system	orthorhombic	orthorhombic	monoclinic	triclinic
Space group	*Pnma*	*Pnma*	*C*2	$P\bar{1}$
a/Å	17.9992(2)	17.65820(10)	29.9712(5)	17.0853(1)
b/Å	23.8500(2)	23.6916(2)	17.2882(3)	17.1129(1)
c/Å	18.1211(2)	18.15350(10)	17.9740(3)	34.9475(3)
α/°	90	90	90	89.480(1)
β/°	90	90	93.570(2)	82.341(1)
γ/°	90	90	90	60.059(14)
V/Å^3	7779.04(14)	7594.54(9)	9295.1(3)	8755.59(14)
Z	4	4	4	4
ρ_{calc} (g/cm^3)	1.485	1.580	1.377	1.483
F(000)	3536	3632	3951.843	3883.171
Reflections collected	48843	37386	105765	265385
Independent reflections	7082	7573	105765	33773
R_{int} (%)	0.0584	0.0542	—	0.0680
GOF on F^2	1.070	1.213	0.9947	1.0433
R_1[a]	0.0546	0.0465	0.0670	0.0567
wR_2[b]	0.1569	0.1166	0.1688	0.1435

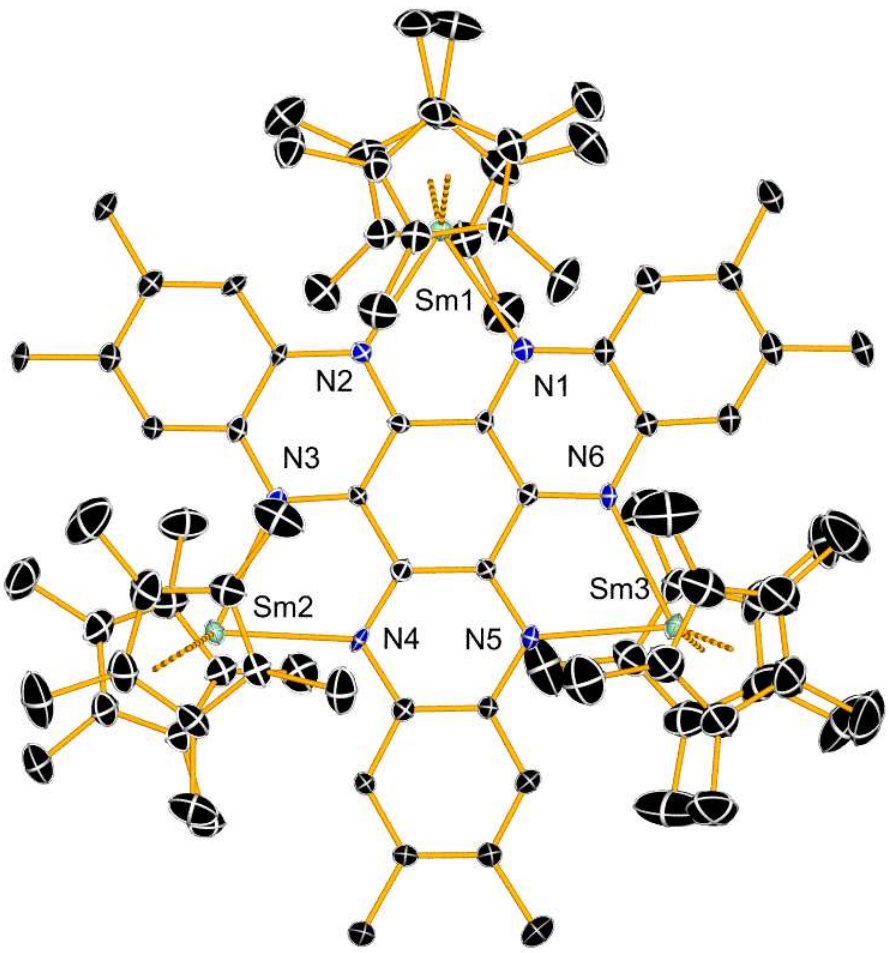

Figure S1. Molecular structure of **2**$_{Sm}$. Thermal ellipsoids are set to 50 % probability. Atoms in grey are carbon, blue are nitrogen and green are Samarium. Solvent molecules and hydrogen atoms are omitted for clarity.

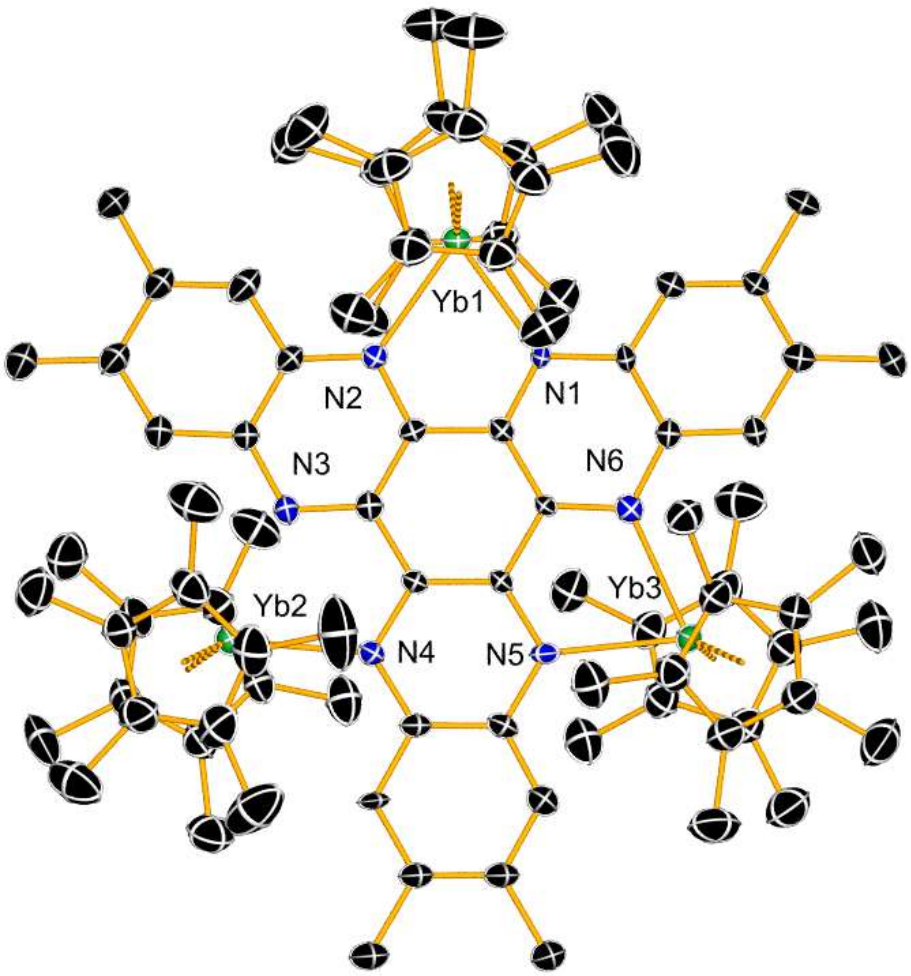

Figure S2. Molecular structure of **1**$_{Yb}$. Thermal ellipsoids are set to 50 % probability. Atoms in grey are carbon, blue are nitrogen and green are ytterbium. Disorder components are shown 'ghosted' atoms, and solvent molecules and hydrogen atoms are omitted for clarity.

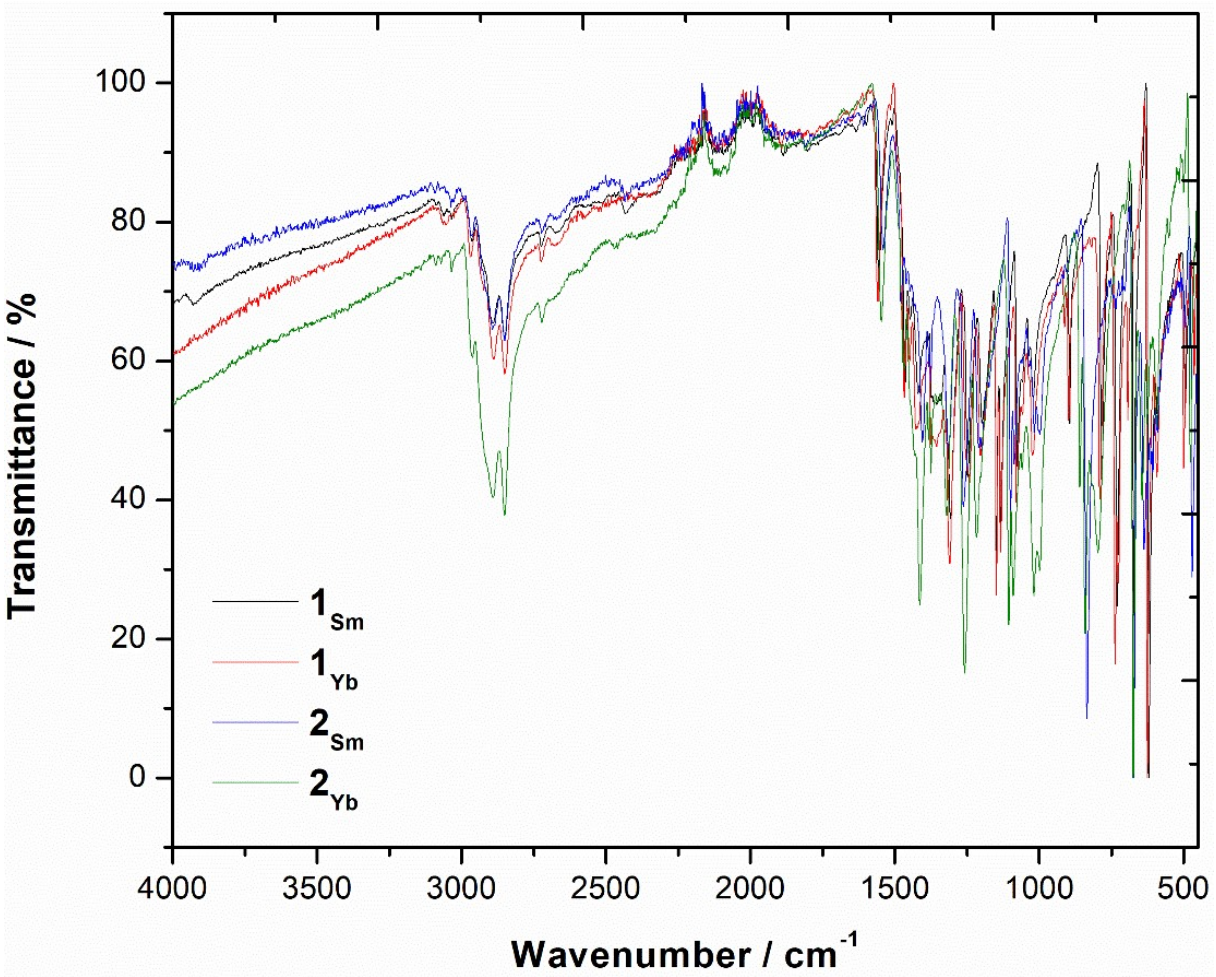

Figure S3. FTIR spectra of $\mathbf{1}_{Sm}\cdot C_7H_8$ (black), $\mathbf{1}_{Yb}\cdot C_7H_8$ (red), $\mathbf{2}_{Sm}\cdot 0.5(C_6H_6)$ (blue) and $\mathbf{2}_{Yb}\cdot 0.5(C_6H_6)$ (green).

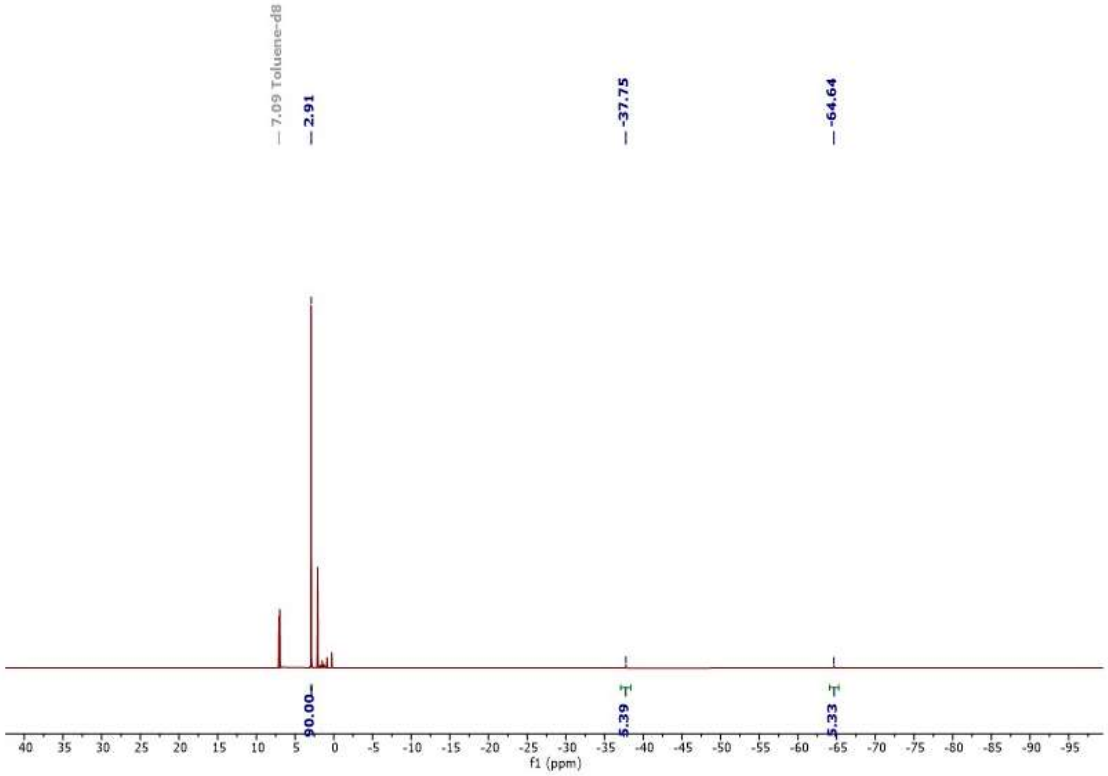

Figure S4. ^{1}H NMR spectrum of **1$_{Sm}$**·C_7H_8 in toluene-D_8 at 300 K.

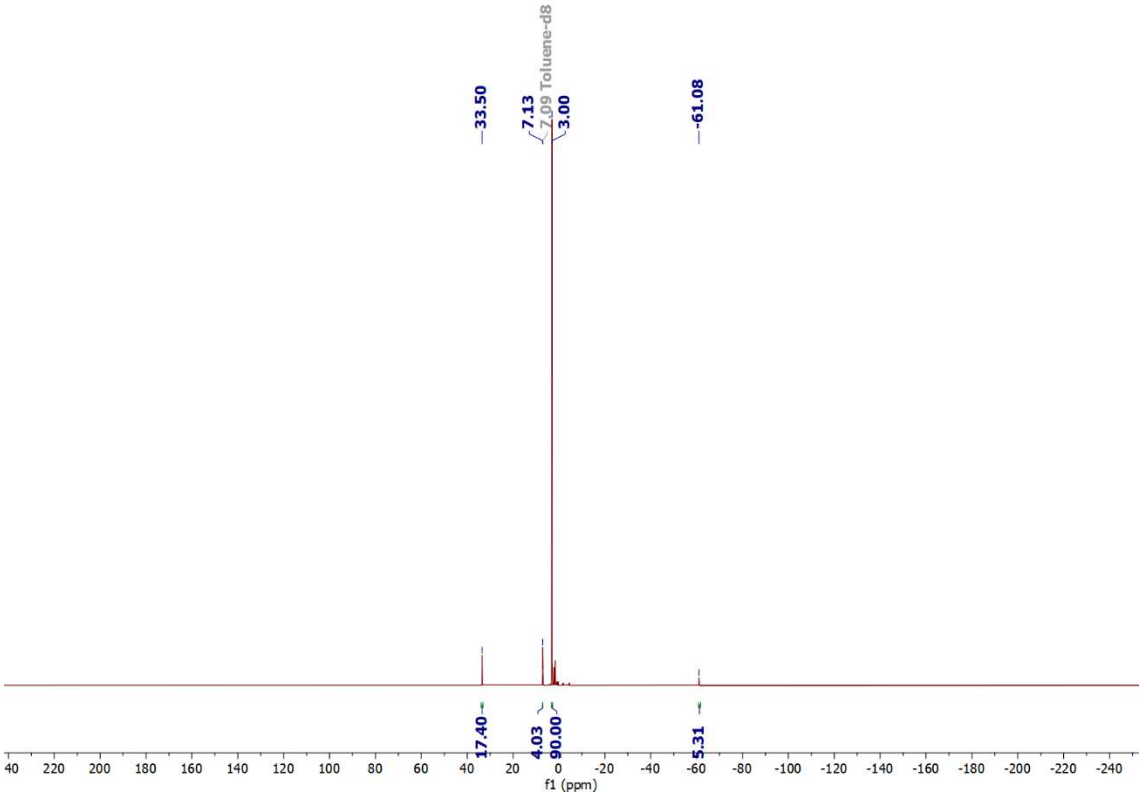

Figure S5. ^{1}H NMR spectrum of **2$_{Sm}$**·0.5(C_6H_6) in toluene-D_8 at 300 K.

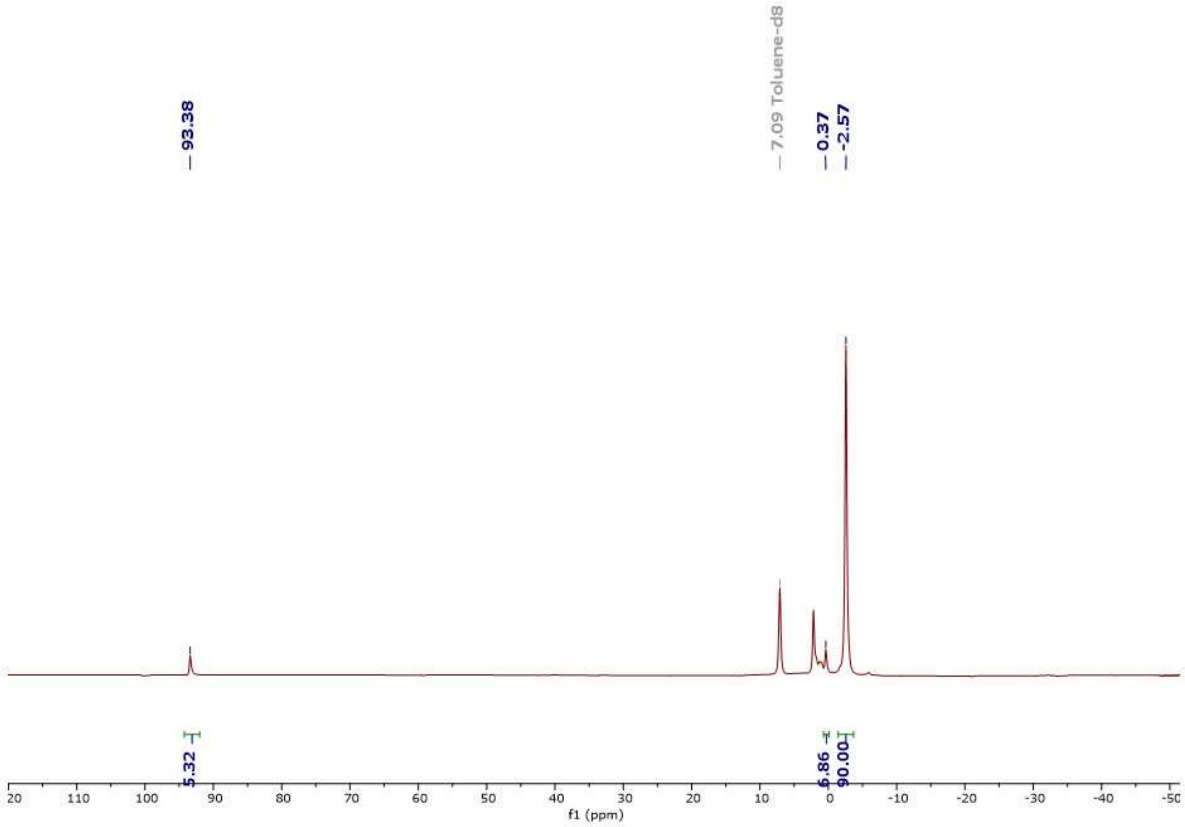

Figure S6. ^{1}H NMR spectrum of **1**$_{Yb}$·C_7H_8 in toluene-D_8 at 300 K.

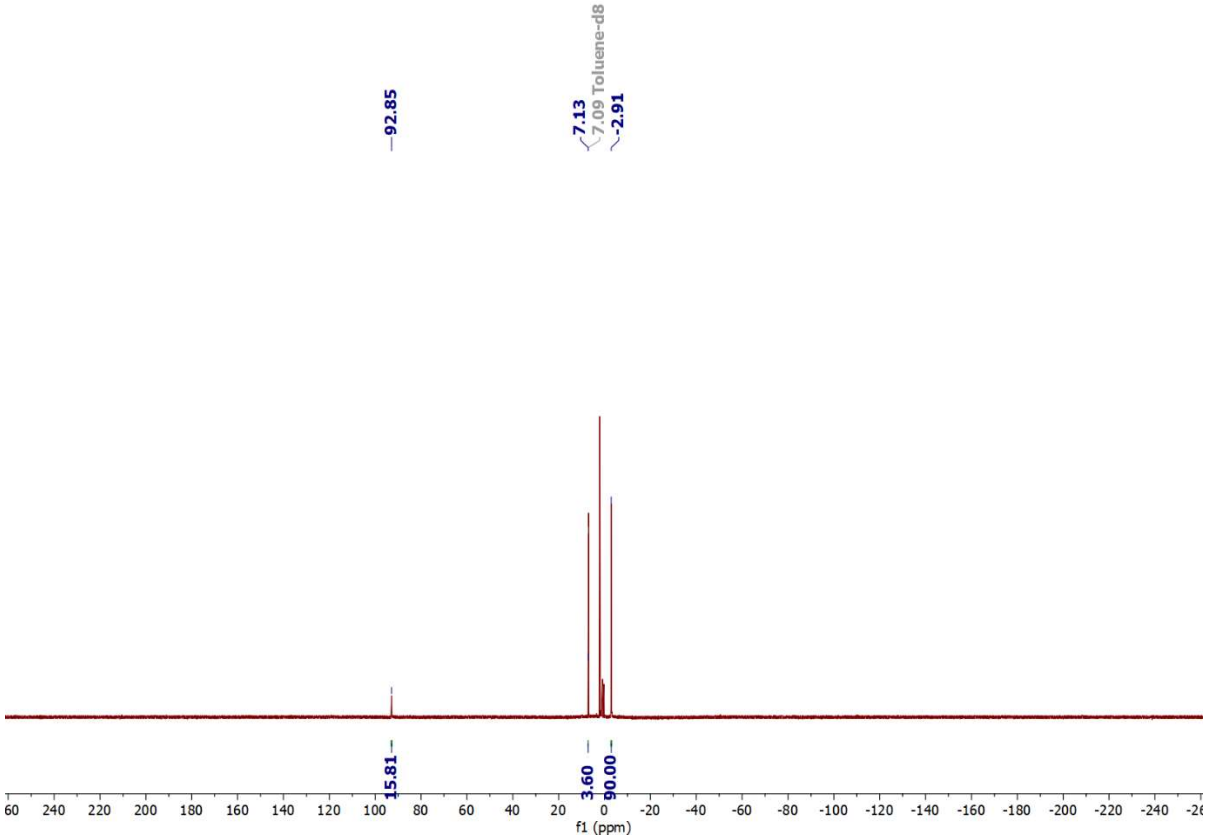

Figure S7. ^{1}H NMR spectrum of **2**$_{Yb}$·0.5(C_6H_6) in toluene-D_8 at 300 K.

Variable Temperature ^{1}H NMR spectra

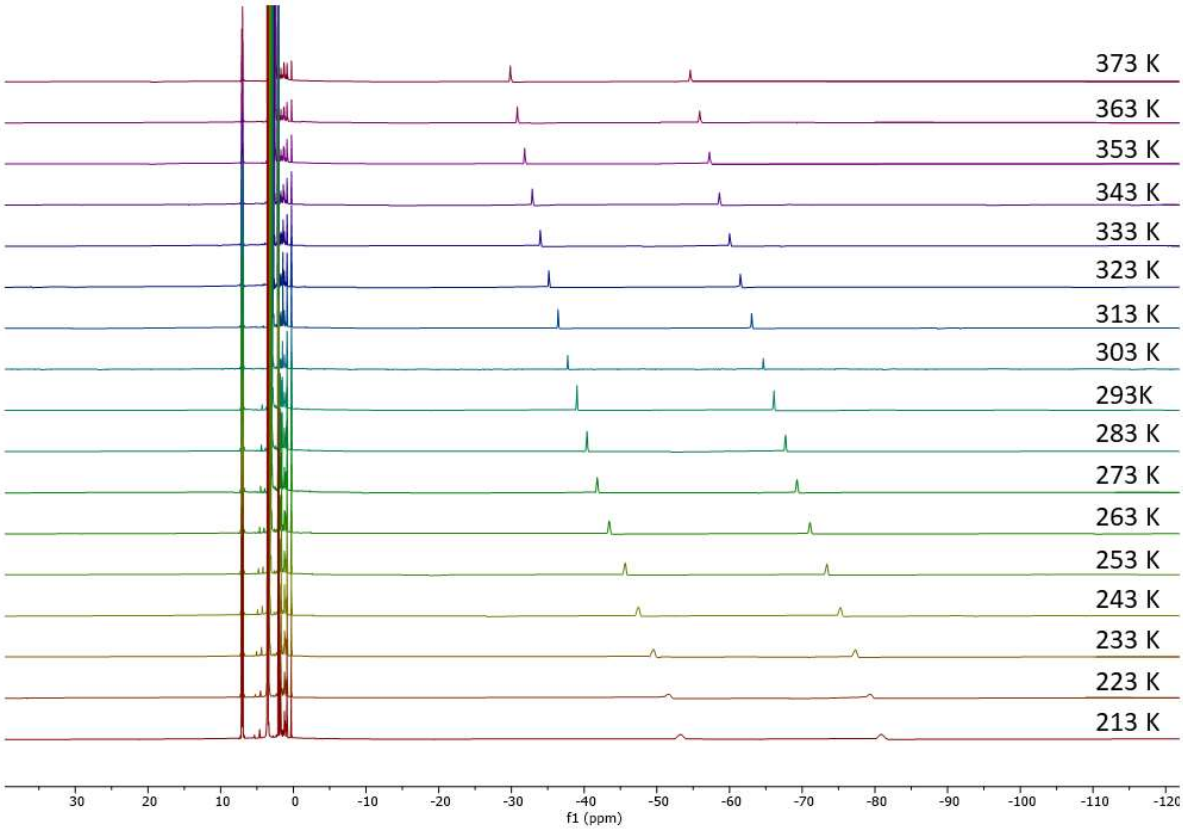

Figure S8. Variable-temperature ^{1}H NMR spectra of **1$_{Sm}$**·C_7H_8 in toluene-D_8.

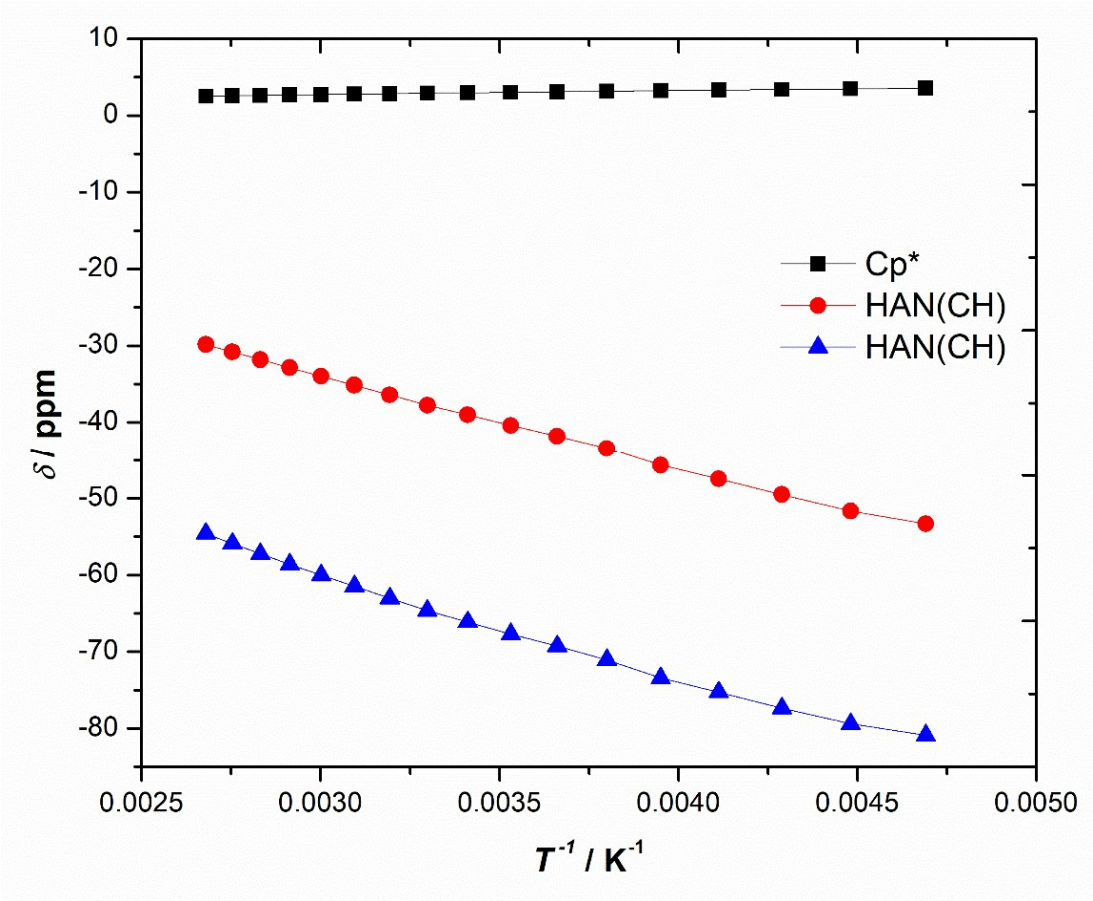

Figure S9. Temperature dependence of the ^{1}H chemical shift for $\mathbf{1_{Sm}}\cdot C_7H_8$, plotted as δ vs T^{-1} at temperatures in the range 213-373 K at intervals of 10 K.

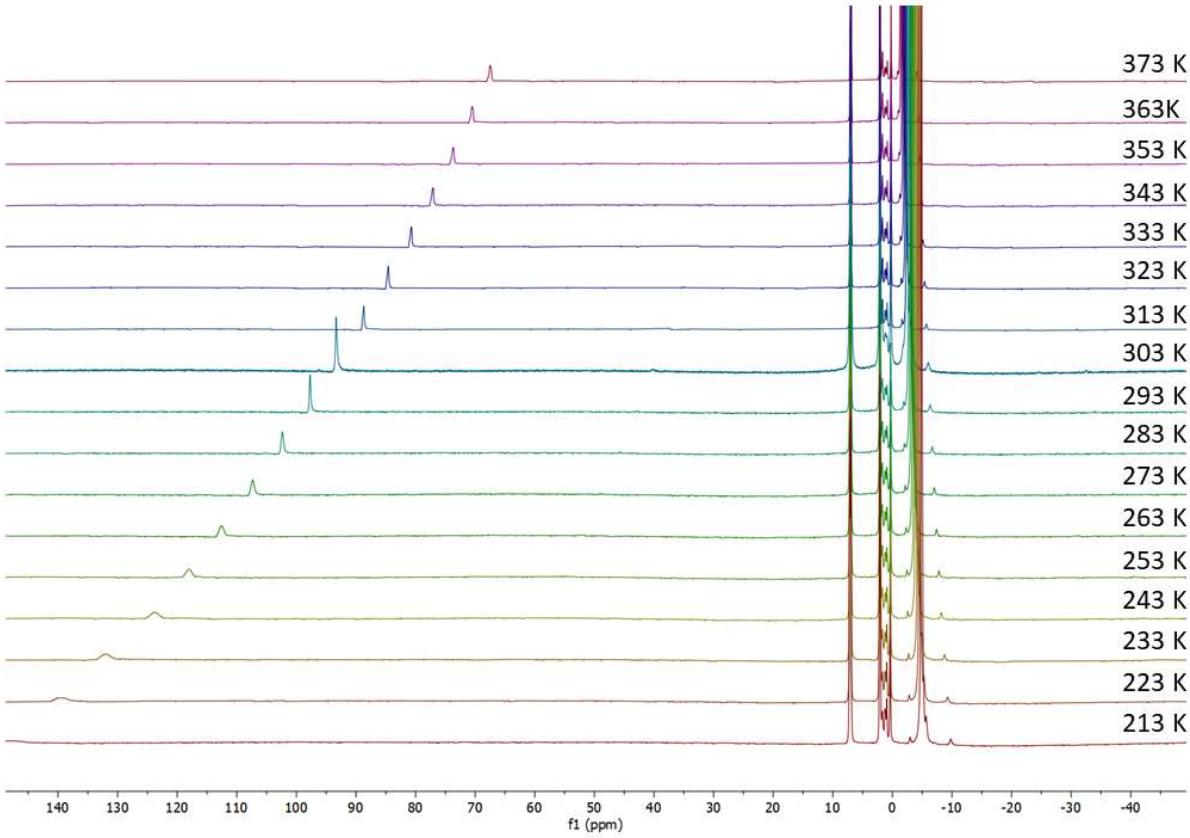

Figure S10. Variable-temperature ^{1}H NMR spectra of $\mathbf{1_{Yb}}\cdot C_7H_8$ in toluene-D_8.

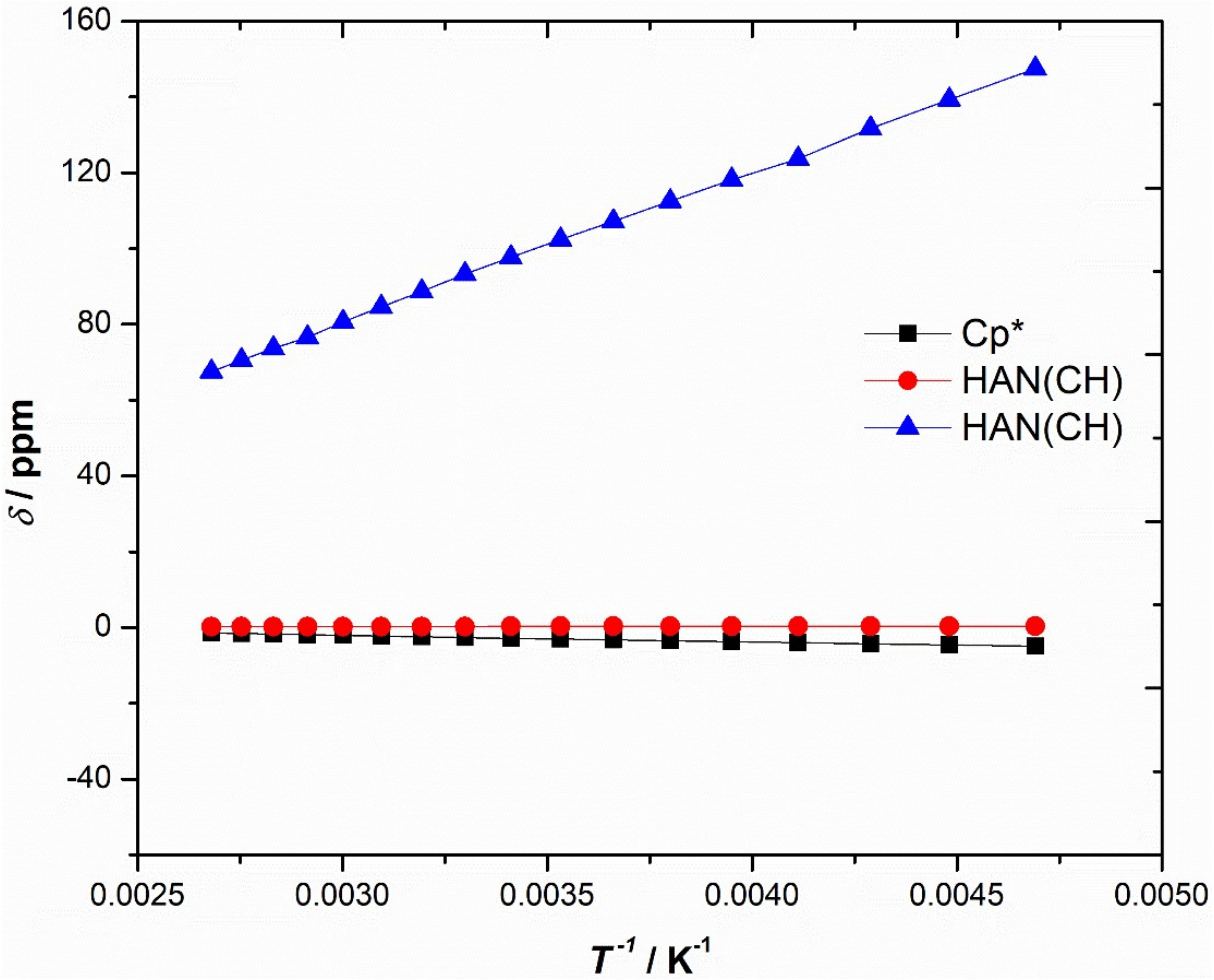

Figure S11. Temperature dependence of the ^{1}H chemical shift for $\mathbf{1}_{Yb}\cdot C_7H_8$, plotted as δ vs T^{-1} at temperatures in the range 213-373 K at intervals of 10 K.

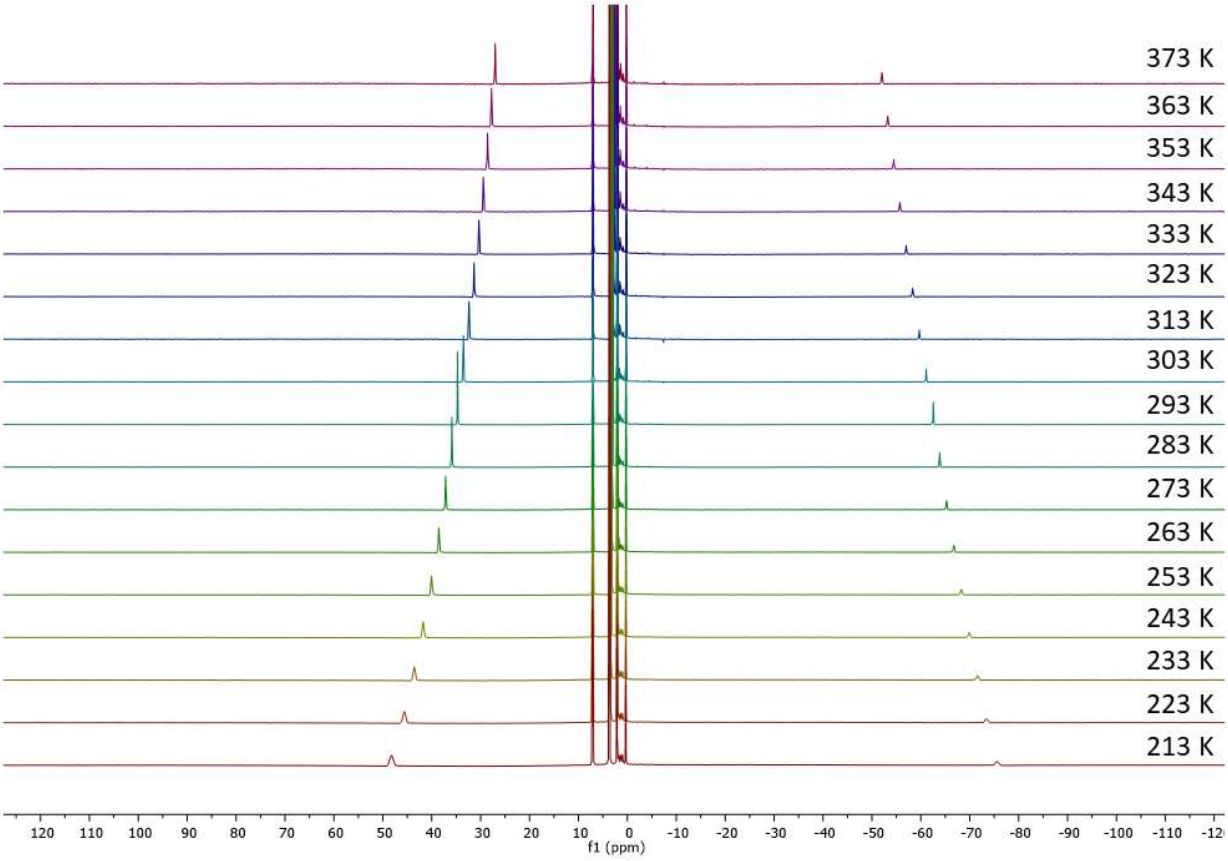

Figure S12. Variable-temperature ^{1}H NMR spectra of $\mathbf{2_{Sm}}\cdot 0.5(C_6H_6)$ in toluene-D_8.

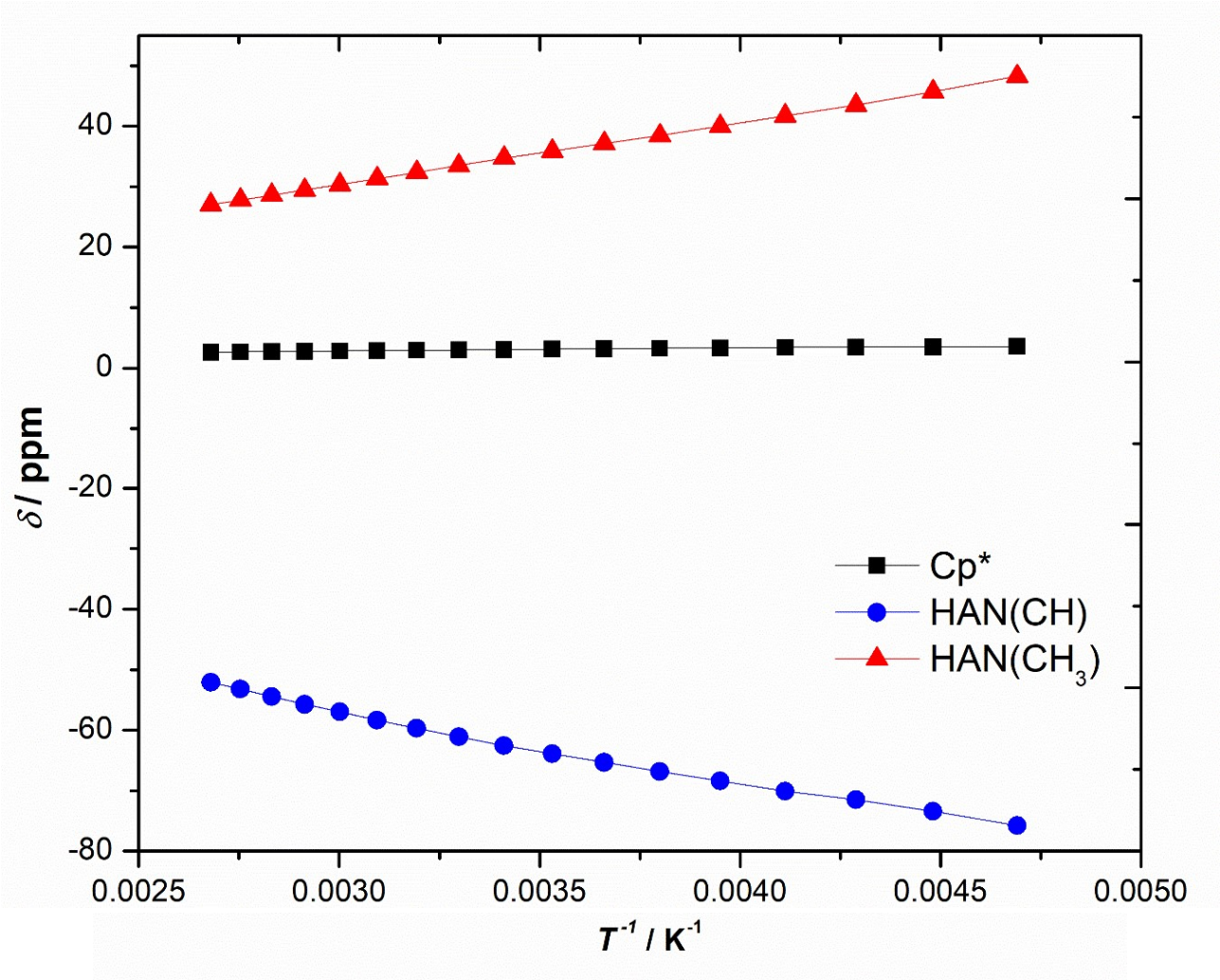

Figure S13. Temperature dependence of the ^{1}H chemical shift for $\mathbf{2}_{\mathbf{Sm}}$·0.5(C_6H_6), plotted as δ vs T^{-1} at temperatures in the range 213-373 K at intervals of 10 K.

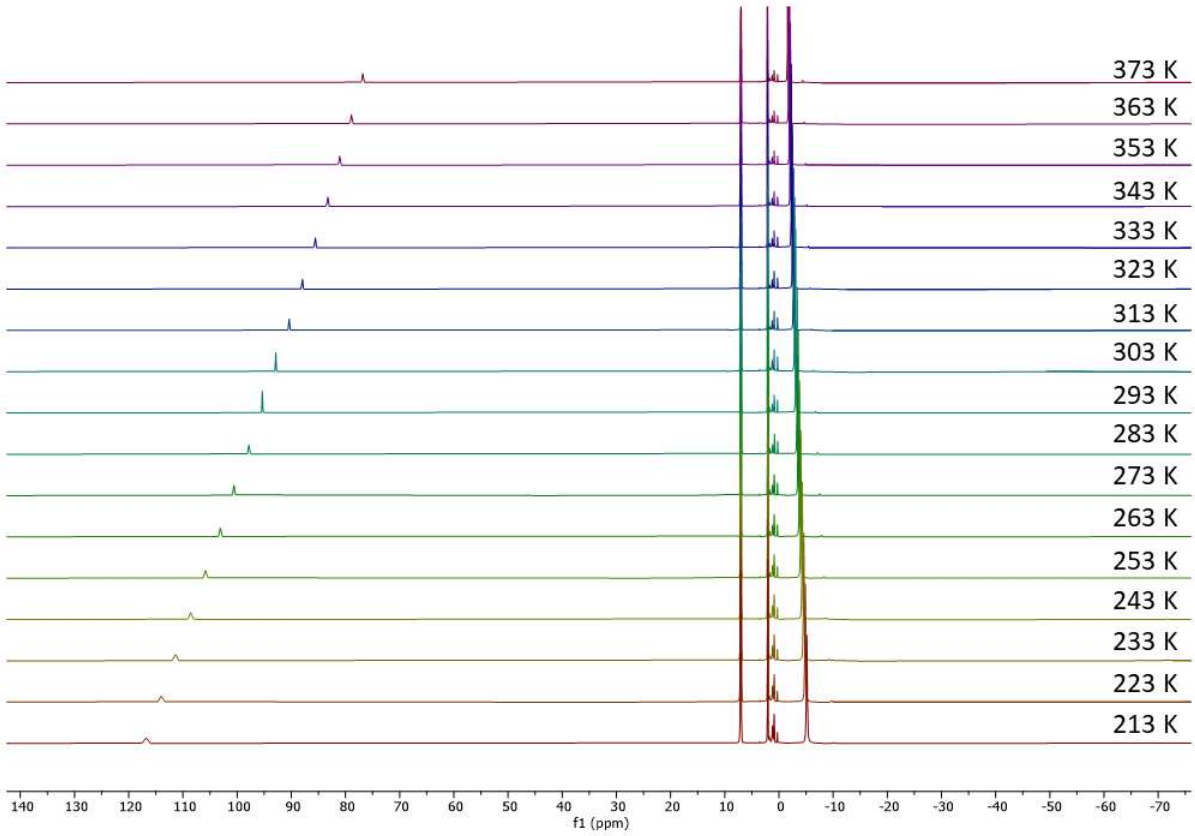

Figure S14. Variable-temperature ^{1}H NMR spectra of $\mathbf{2_{Yb}}\cdot 0.5(C_6H_6)$ in toluene-D_8.

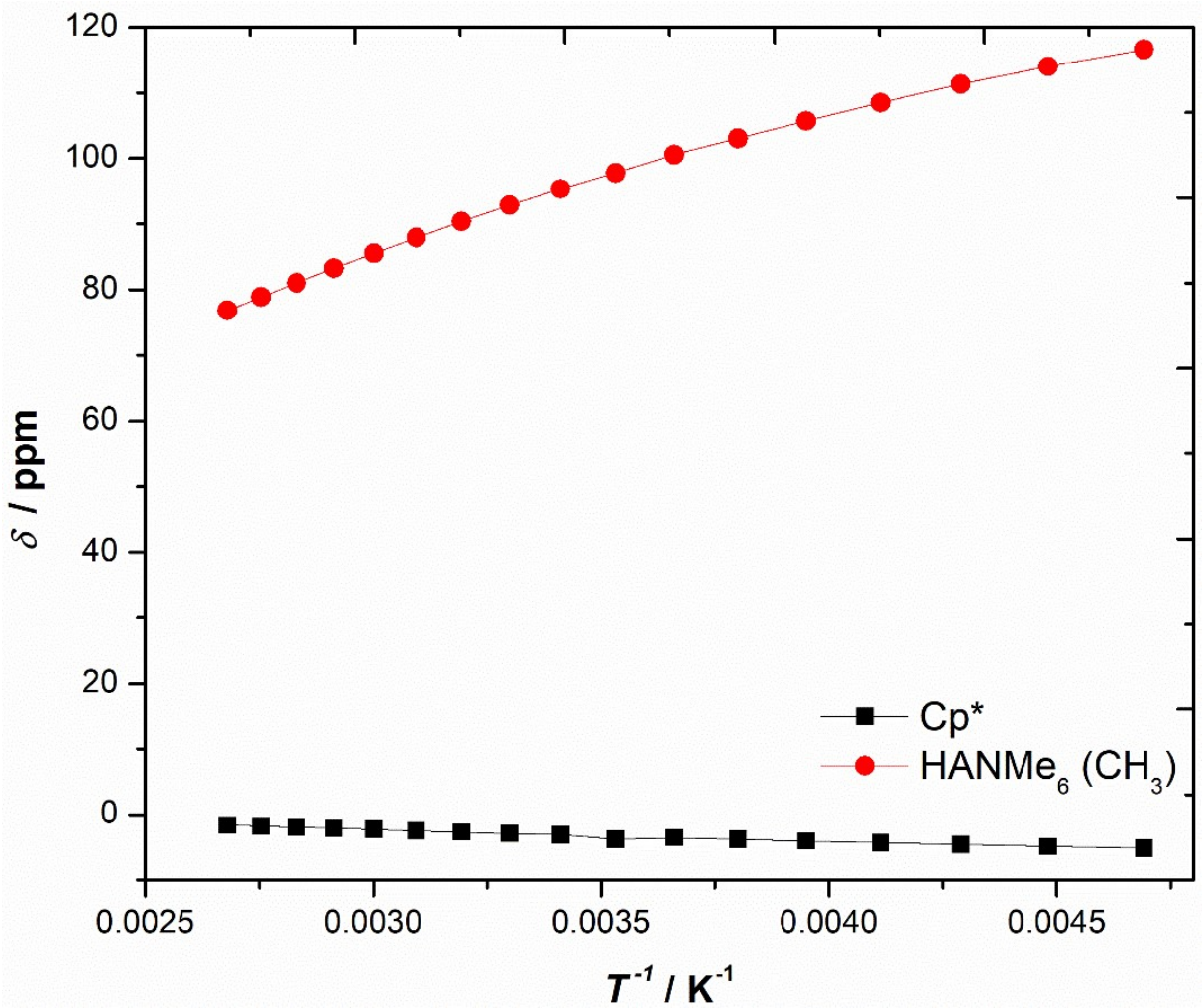

Figure S15. Temperature dependence of the ^{1}H chemical shift for $\mathbf{2}_{\mathbf{Yb}}$·0.5(C_6H_6), plotted as δ vs T^{-1} at temperatures in the range 213-373 K at intervals of 10 K.

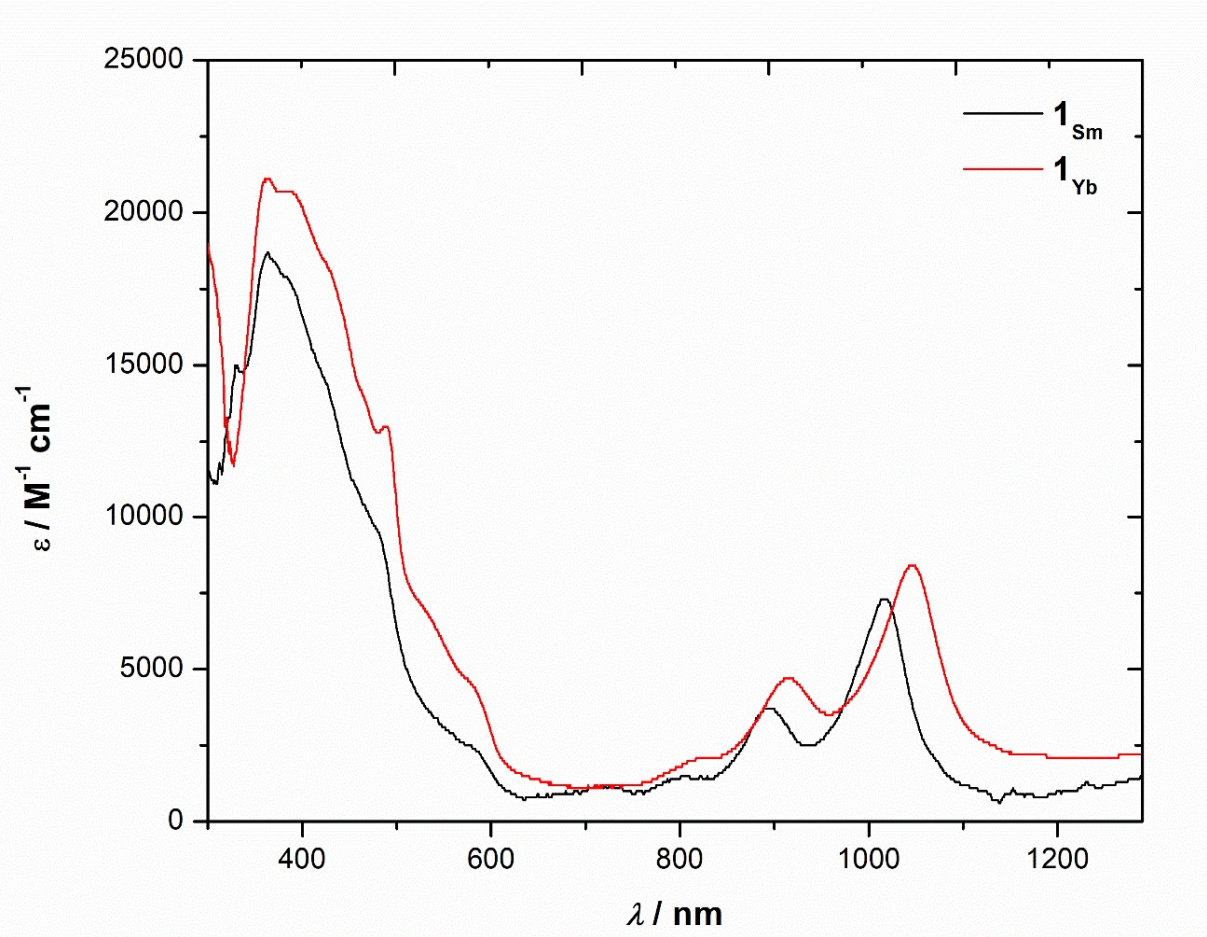

Figure S16. UV/vis/NIR spectra of $\mathbf{1_{Sm}}\cdot C_7H_8$ (black) and $\mathbf{1_{Yb}}\cdot C_7H_8$ (red) in toluene (0.1 mM).

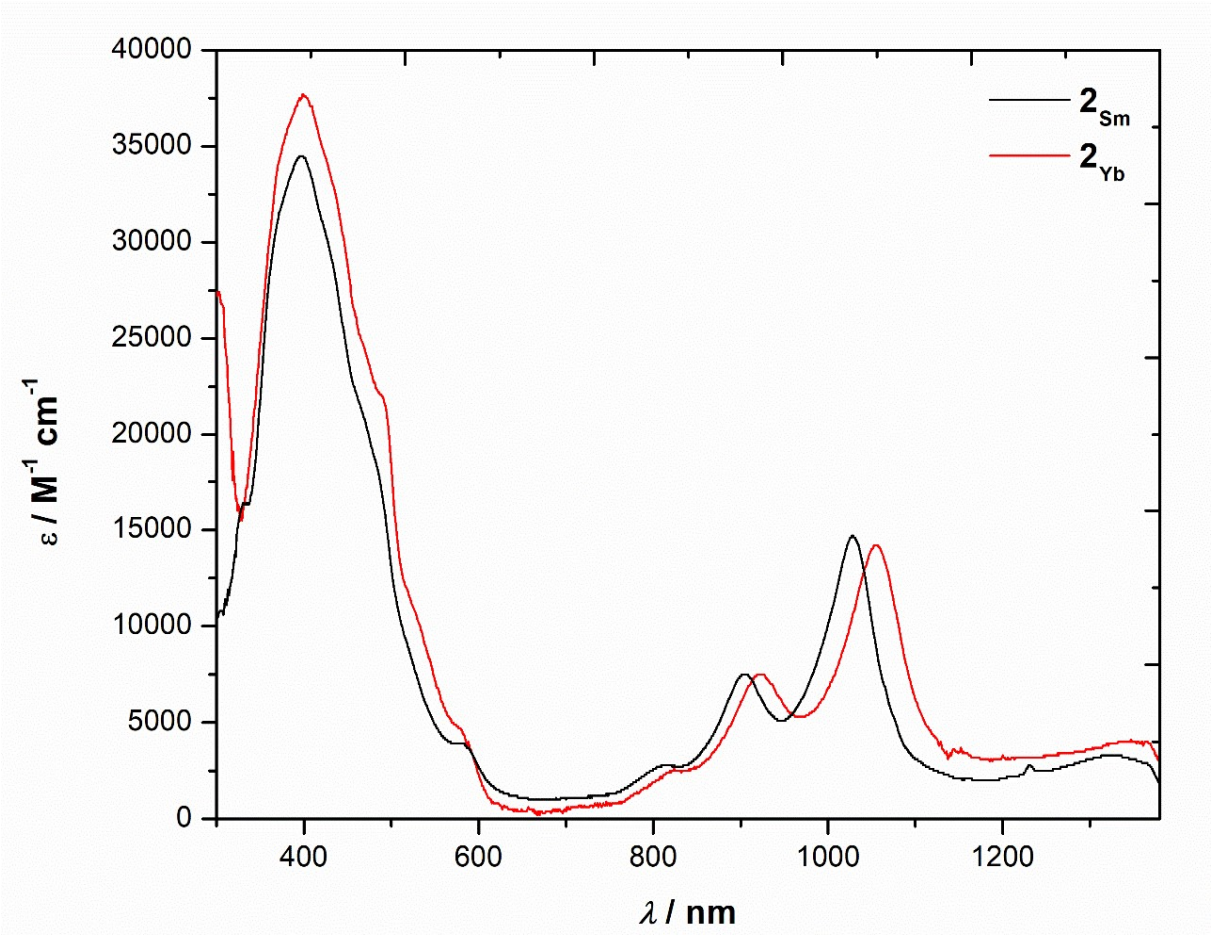

Figure S17. UV/vis/NIR spectra of $\mathbf{2}_{Sm}$·0.5(C_6H_6) (black) and $\mathbf{2}_{Yb}$·0.5(C_6H_6) (red) in toluene (0.1 mM).

Magnetic Property Measurements

Magnetic measurements were recorded on a quantum design MPMS-XL7 SQUID magnetometer equipped with a 7 T magnet. Samples were restrained in eicosane and sealed in 7 mm NMR tubes. Direct current magnetic susceptibility measurements were performed on samples, in an applied field of 1000 Oe with temperature range 1.9-300 K. Diamagnetic corrections were calculated using Pascals constants.[7]

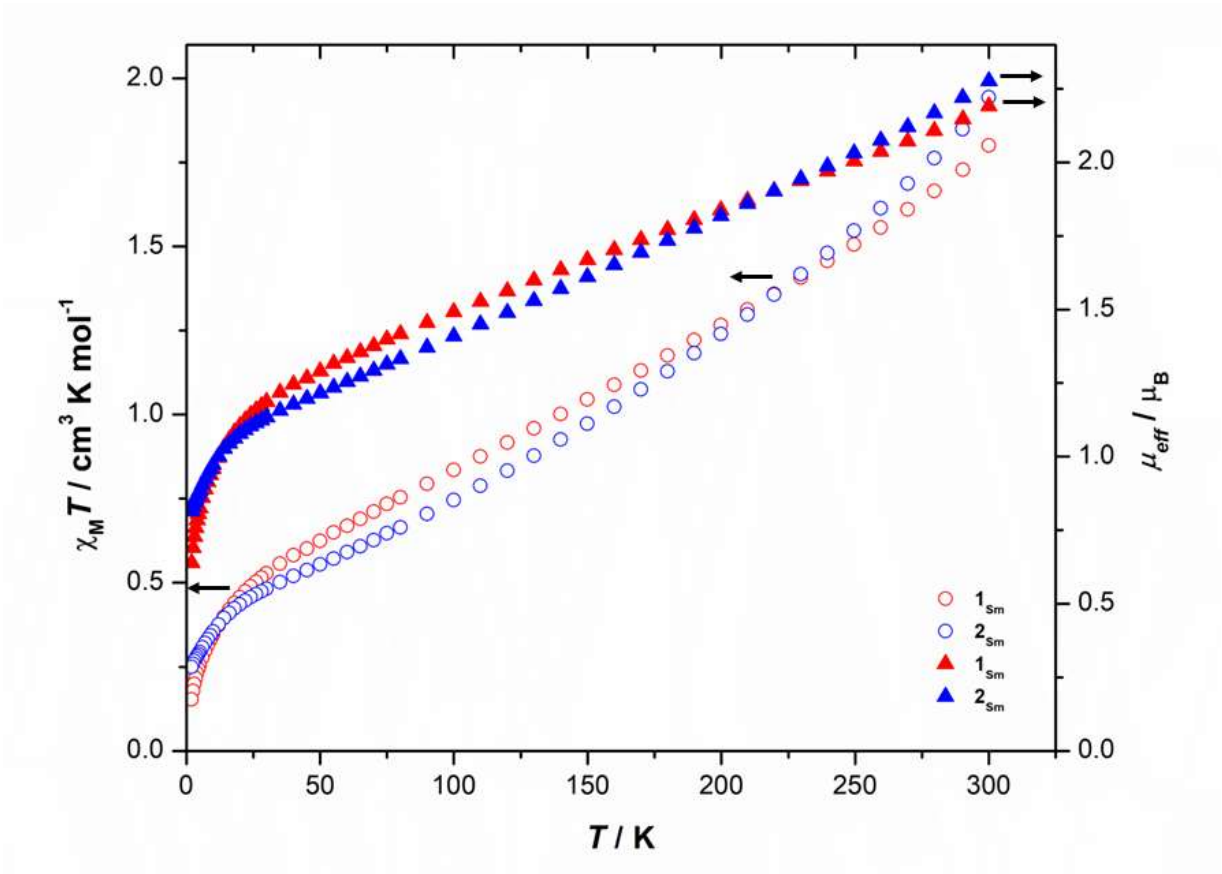

Figure S18. $\chi_M T$ vs. T (circular data points) and μ_{eff} vs. T (triangular data points) for **1**$_{Sm}$·C_7H_8 (red) and **2**$_{Sm}$·0.5(C_6H_6) (blue).

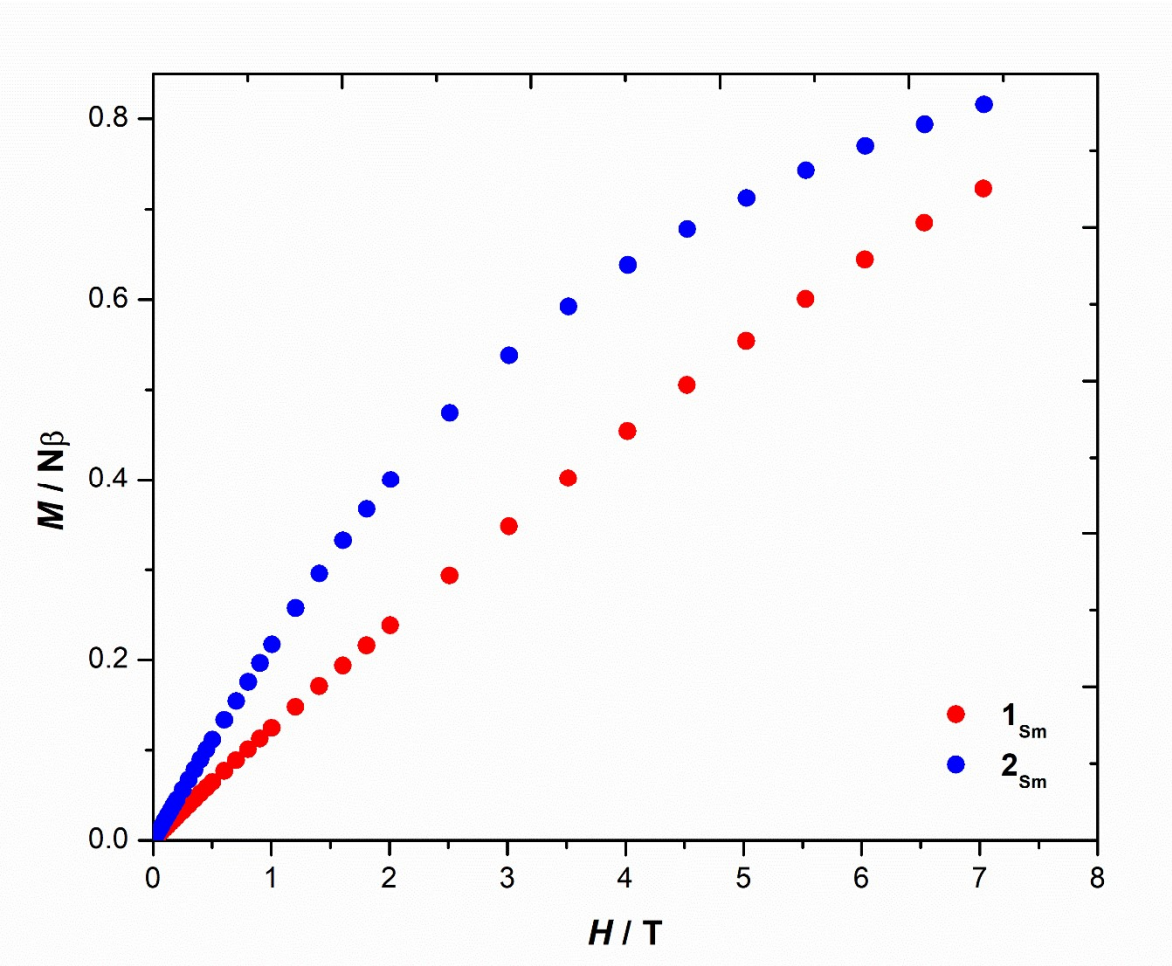

Figure S19. Magnetization (*M*) vs. magnetic field (*H*) for $\mathbf{1}_{Sm}\cdot C_7H_8$ (red) and $\mathbf{2}_{Sm}\cdot 0.5(C_6H_6)$ (blue) at 1.9 K.

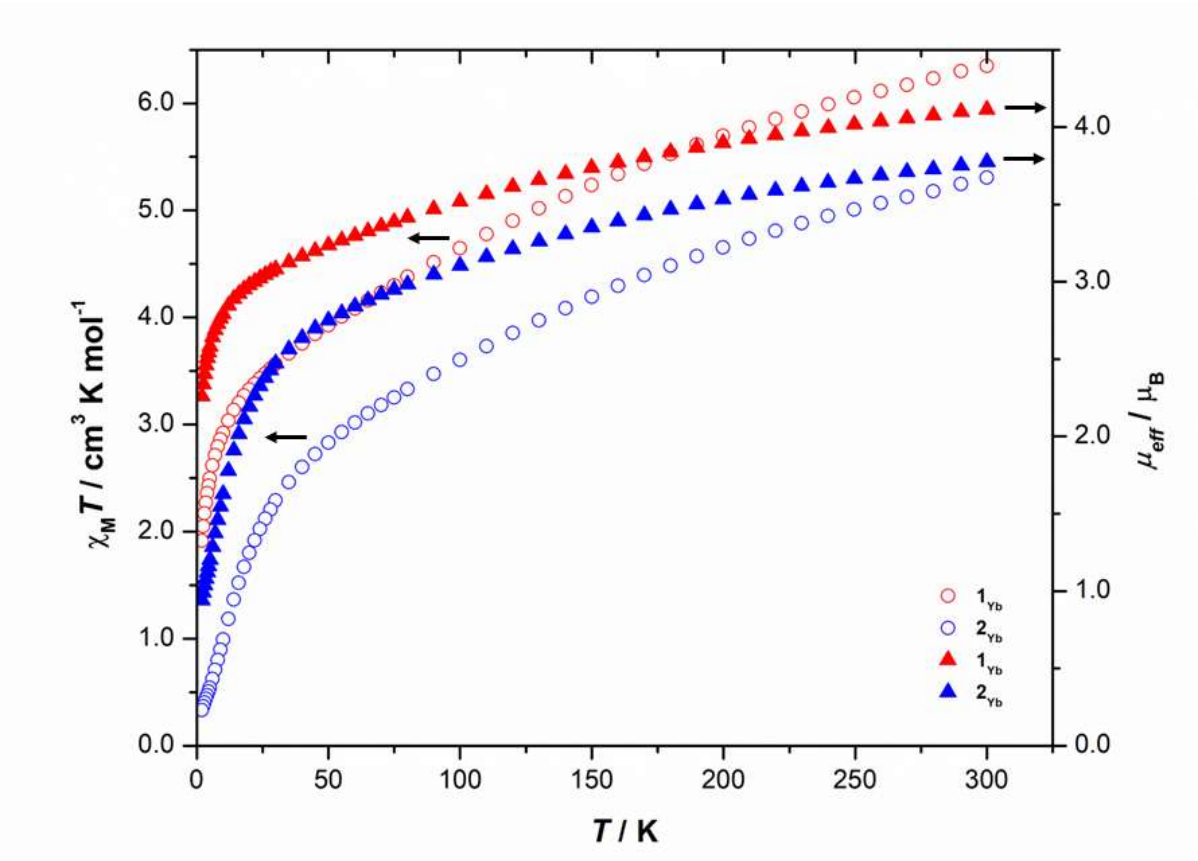

Figure S20. $\chi_M T$ vs. T (circular data points) and μ_{eff} vs. T (triangular data points) for **1**$_{Yb}$·C_7H_8 (red) and **2**$_{Yb}$·0.5(C_6H_6) (blue).

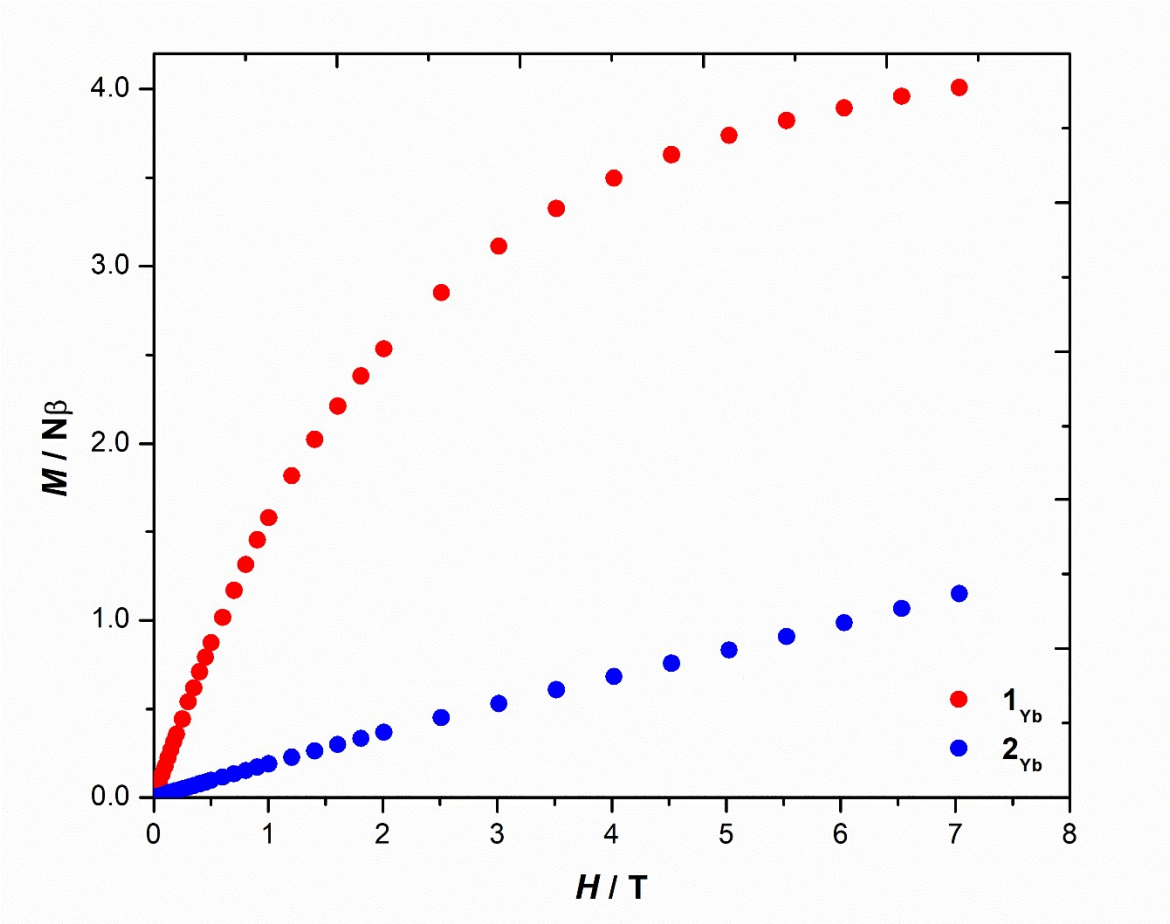

Figure S21. Magnetization (*M*) vs. magnetic field (*H*) for **1**$_{Yb}$·C_7H_8 (red) and **2**$_{Yb}$·0.5(C_6H_6) (blue) at 1.9 K.

Computational Details

The geometries of $\mathbf{1}_{\mathbf{Sm}}$ and $\mathbf{1}_{\mathbf{Yb}}$ were extracted from their respective crystal structures. The positions of hydrogen atoms were optimized while the positions of heavier atoms were frozen to their crystal-structure coordinates. The geometry optimizations were carried out using density functional theory (DFT) as implemented in the *Gaussian 16* software revision C.02.[8] The range-separated hybrid CAM-B3LYP exchange-correlation functional[9] was used in all DFT calculations. To avoid complications that arise from the strong degeneracies within the 4*f* shell, the 4*f* electrons were treated with 4*f*-in-core pseudopotentials with corresponding valence-polarized basis sets.[10] The Stuttgart-type MWB51 and MWB59 pseudopotentials were used for $\mathbf{1}_{\mathbf{Sm}}$ and $\mathbf{1}_{\mathbf{Yb}}$, respectively, which treat 51 and 59 electrons as part of the pseudopotential. The remaining atoms were treated with valence-polarized double-ζ def2-SVP basis sets.[11] Consecutive single-point calculations were carried out at the same level of theory. Stability analyses[12] were carried out to ensure that the wave functions correspond to minima in the molecular orbital coefficient space.

Multireference calculations were carried out with the *Orca* software version 5.0.4.[13] The calculations correlated the 4*f* electrons of one ion and the three electrons from the $[HAN]^{3-}$ anion. The remaining two ions in each calculation were replaced by diamagnetic Y(III) ions. Two of the lanthanide ions in both structures are crystallographically equivalent, so the calculations were carried out on the two nonequivalent ions in separately in the case of each structure. First, state-averaged (SA) complete active space self-consistent field (CASSCF) calculations[14] were carried out. The orbital space consisted of the seven 4*f* orbitals and three $[HAN]^{3-}$ orbitals. In the case of $\mathbf{1}_{\mathbf{Sm}}$, 8 electrons were correlated and in case of $\mathbf{1}_{\mathbf{Yb}}$, 16 electrons. The number of roots solved in the SA calculations was based on a trial-and-error procedure to select entire groups of manifolds of states. In the case of $\mathbf{1}_{\mathbf{Sm}}$, 18, 124, 124, 66 and 48 states with spins $S = 9$, $S = 7$, $S = 5$, $S = 3$ and $S = 1$, respectively, were chosen that correspond to a rough energy cutoff of 23,000 cm^{-1}. In the case of $\mathbf{1}_{\mathbf{Yb}}$, 7, 63 and 56 states with respective spins $S = 5$, $S = 3$ and $S = 1$ were chosen that correspond to a rough energy cutoff of 34,000 cm^{-1}. The energy cutoffs were chosen at places where there is a natural discontinuity of the energy spectrum. Electron correlation effects outside the active space were estimated using the second-order *N*-electron valence-state perturbation theory (NEVPT2) in its strongly contracted formulation.[15]

Spin-orbit coupling was introduced using the quasi-degenerate perturbation theory (QDPT) approach where the spin-orbit coupled Hamiltonian is constructed in the basis of the CASSCF eigenstates and diagonalized to yield the spin-orbit coupled states.[16] The operator was constructed using the spin-orbit mean-field (SOMF) method.[17] The NEVPT2 correction was taken into account as energy shifts in the diagonal values of the Hamiltonian, whereas the off-diagonal elements were calculated purely on the basis of the SA-CASSCF eigenstates. Scalar relativistic effects were introduced using the standard second-order Douglas–Kroll–Heß (DKH) transformation.[18] The valence-polarized triple-ζ SARC-DKH-TZVP basis sets[19] were used for the lanthanides, valence-polarized double-ζ DKH-def2-SVP basis sets were used for the C and N atoms, and the plain double-ζ DKH-def2-SV basis set was used for H atoms.[11,20]

Table S2. Energies and <S^2> expectation values calculated at the DFT level (using 4*f*-in-core pseudopotentials) for the different spin states of $\mathbf{1}_{Sm}$ and $\mathbf{1}_{Yb}$.

	Energy / Hartree atomic units		<S^2>	
	Doublet	Quartet	Doublet	Quartet
$\mathbf{1}_{Sm}$	–3690.69330016	–3690.69598751	1.6180	3.7896
$\mathbf{1}_{Yb}$	–3704.83600679	–3704.83873506	1.6225	3.7888

Table S3. Energies (in cm^{-1}) of low-lying CASSCF eigenstates calculated for $\mathbf{1}_{Sm}$.

Sm1			Sm2		
Root index	Multiplicity	Energy	Root index	Multiplicity	Energy
0	5	0.0	0	5	0.0
0	7	1.0	0	7	1.0
0	5	1.8	0	5	1.8
0	3	2.4	0	3	2.4
1	3	20.2	1	3	20.2
1	5	21.8	1	5	21.8
1	7	23.5	1	7	23.5
1	9	24.6	1	9	24.6
2	9	460.2	2	9	460.2
2	7	468.2	2	7	468.2
2	5	474.1	2	5	474.1
2	3	478.1	2	3	478.1
3	9	536.2	3	9	536.2
3	7	543.7	3	7	543.7
4	9	545.2	4	9	545.2
3	5	548.5	3	5	548.5
4	7	549.7	4	7	549.7
3	3	551.3	3	3	551.3
4	5	553.1	4	5	553.1
4	3	555.4	4	3	555.4
5	3	646.6	5	3	646.6
6	3	653.2	6	3	653.2
5	5	664.3	5	5	664.3
6	5	671.2	6	5	671.2
5	7	691.0	5	7	691.0
6	7	698.2	6	7	698.2
5	9	726.9	5	9	726.9
6	9	734.5	6	9	734.5
7	3	783.5	7	3	783.5
7	5	796.9	7	5	796.9
7	7	818.0	7	7	818.0
8	3	837.3	8	3	837.3
7	9	847.3	7	9	847.3
8	5	847.5	8	5	847.5
8	7	863.7	8	7	863.7
8	9	886.5	8	9	886.5

Table S4. Energies (in cm^{-1}) of low-lying CASSCF eigenstates calculated for $\mathbf{1}_{Yb}$.

Yb1			Yb2		
Root index	Multiplicity	Energy	Root index	Multiplicity	Energy
0	3	0.0	0	3	0.0
0	5	82.7	0	5	79.3
1	5	233.6	1	5	232.5
1	3	253.5	1	3	252.5
2	5	398.8	2	5	370.3
2	3	413.1	2	3	384.9
3	3	542.7	3	3	515.1
3	5	550.3	3	5	520.8
4	5	842.4	4	5	794.4
4	3	853.4	5	5	803.2
5	5	855.3	4	3	805.4
5	3	865.3	5	3	813.3
6	5	944.3	6	5	898.4
6	3	954.1	6	3	908.7

Table S5. NEVPT2-corrected energies (in cm^{-1}) of low-lying CASSCF eigenstates calculated for $\mathbf{1}_{Sm}$.

Sm1			Sm2		
Root index	Multiplicity	Energy	Root index	Multiplicity	Energy
11	5	0.0	11	5	0.0
11	7	13.9	11	7	13.9
12	5	47.2	12	5	47.2
12	7	61.9	12	7	61.9
15	5	328.0	15	5	328.0
15	7	336.6	15	7	336.5
13	5	357.1	13	5	357.0
13	7	390.1	13	7	390.0
14	5	401.1	14	5	401.1
14	7	431.9	14	7	431.9
16	5	453.1	16	5	453.1
16	7	455.3	16	7	455.2
17	5	464.0	17	5	464.0
17	7	470.9	17	7	470.8
19	5	622.0	19	5	622.0
18	5	641.4	18	5	641.4
19	7	666.9	19	7	666.9
18	7	681.6	18	7	681.6
21	5	694.0	21	5	693.9
54	5	733.0	54	5	732.5
54	7	745.6	54	7	745.1
21	7	746.0	21	7	745.9
55	5	765.8	55	5	765.3
20	5	772.4	20	5	772.4
22	5	774.4	22	5	774.4
55	7	789.8	55	7	789.3
23	5	806.1	23	5	806.1
22	7	808.6	22	7	808.6
20	7	811.9	20	7	811.9
24	5	821.2	24	5	821.2
23	7	856.9	23	7	856.9
24	7	860.8	24	7	860.8
56	5	908.4	56	5	908.7
26	5	933.8	26	5	933.8
28	5	940.9	28	5	940.9
56	7	943.2	56	7	943.5

57	5	951.7	57	5	952.0
27	5	960.7	27	5	960.6
25	7	965.7	25	7	965.7
26	7	974.9	26	7	974.9
25	5	978.4	25	5	978.4
57	7	990.5	57	7	990.7

Table S6. NEVPT2-corrected energies (in cm^{-1}) of low-lying CASSCF eigenstates calculated for $\mathbf{1}_{Yb}$.

Yb1 ion			Yb2 ion		
Root index	Multiplicity	Energy	Root index	Multiplicity	Energy
35	1	0.0	35	1	0.0
42	3	9.5	42	3	16.9
43	3	360.8	37	1	293.9
36	1	379.7	44	3	293.9
44	3	386.6	43	3	332.9
37	1	388.1	36	1	334.2
38	1	507.6	38	1	470.5
45	3	542.4	45	3	499.3
46	3	775.6	40	1	716.6
39	1	777.7	46	3	732.5
40	1	814.9	47	3	733.1
47	3	815.0	39	1	750.7
41	1	986.6	41	1	847.1
48	3	989.2	48	3	853.3

Table S7. Energies (in cm^{-1}) of low-lying SOC eigenstates calculated using NEVPT2 and CASSCF diagonal energies for $\mathbf{1}_{Sm}$.

Sm1 ion		Sm2 ion	
CASSCF	NEVPT2	CASSCF	NEVPT2
0.00	0.00	0.00	0.00
0.30	1.80	0.30	1.81
0.42	11.27	0.42	11.27
4.39	11.53	4.39	11.53
4.41	360.79	4.41	360.76
5.93	361.01	5.93	360.99
6.10	381.73	6.10	381.71
6.38	383.41	6.38	383.39
459.61	384.70	459.61	384.68
459.81	387.78	459.82	387.76
460.34	395.20	460.34	395.17
462.51	398.44	462.51	398.40
462.56	553.86	462.56	553.84
467.39	561.76	467.39	561.75
467.42	563.16	467.42	563.15
468.05	576.82	468.05	576.80
640.99	728.65	640.99	728.19
641.09	731.76	641.09	731.29
644.63	738.62	644.63	738.56
647.47	742.93	647.47	742.46
648.75	743.03	648.75	742.55
660.40	748.52	660.40	748.47
662.50	761.49	662.50	761.43
662.97	771.03	662.97	770.99
941.65	784.10	941.65	784.10
941.83	785.18	941.83	785.17
942.16	789.38	942.16	789.36
943.65	790.94	943.65	790.93
943.70	900.37	943.70	900.31
946.47	907.72	946.47	907.97
946.72	908.90	946.72	908.84
946.97	911.48	946.97	911.74
1218.55	915.51	1218.55	915.46
1218.92	936.94	1218.92	937.20
1221.04	937.67	1221.04	937.90

1224.92	937.96	1224.92	937.94

Table S8. Energies (in cm^{-1}) of low-lying SOC eigenstates calculated using NEVPT2 and CASSCF diagonal energies for $\mathbf{1_{Yb}}$.

Yb1 ion		Yb2 ion	
CASSCF	NEVPT2	CASSCF	NEVPT2
0.00	0.00	0.00	0.00
1.75	5.50	1.70	9.78
1.82	6.19	1.78	10.45
46.37	12.83	44.63	10.89
46.37	269.41	44.63	225.02
53.10	281.97	51.19	234.22
53.23	282.90	51.33	234.28
55.08	285.90	53.13	234.50
317.36	582.91	294.15	517.44
317.36	587.31	294.15	519.17
320.67	587.38	297.06	522.38
320.78	587.71	297.32	526.48
322.82	699.59	299.01	629.29
326.86	700.16	303.09	630.41
328.92	701.44	304.85	631.25
328.95	702.25	304.90	635.01
659.48	2468.97	614.40	2364.71
659.84	2493.16	614.76	2406.30
659.97	2493.40	614.91	2406.33
662.95	2493.94	617.71	2407.51
662.96	2664.89	617.72	2566.06
665.42	2723.31	620.32	2592.07
665.61	2725.99	620.49	2592.62
665.96	2726.15	620.84	2592.78
766.61	2782.79	721.65	2666.21
766.62	2789.19	721.66	2671.55
768.25	2789.62	723.46	2671.82
769.02	2816.58	724.17	2672.19
769.92	3023.41	725.26	2840.27
772.21	3025.00	727.37	2843.90
773.39	3030.03	728.73	2844.17
773.44	3032.26	728.77	2845.12

References

1 T. Don Tilley, R. A. Andersen, B. Spencer, H. Ruben, D. H. Templeton and A. Zalkin, *Inorg. Chem.*, 1980, **19**, 2999–3003.

2 W. J. Evans, I. Bloom, W. E. Hunter and J. L. Atwood, *J. Am. Chem. Soc.*, 1981, **103**, 6507–6508.

3 S. Barlow, Q. Zhang, B. R. Kaafarani, C. Risko, F. Amy, C. K. Chan, B. Domercq, Z. A. Starikova, M. Y. Antipin, T. V. Timofeeva, B. Kippelen, J. L. Brédas, A. Kahn and S. R. Marder, *Chem. - A Eur. J.*, 2007, **13**, 3537–3547.

4 G. M. Sheldrick, *Acta Crystallogr. Sect. C Struct. Chem.*, 2015, **C71**, 3–8.

5 O. V. Dolomanov, L. J. Bourhis, R. J. Gildea, J. A. K. Howard and H. Puschmann, *J. Appl. Crystallogr.*, 2009, **42**, 339–341.

6 G. M. Sheldrick, *Acta Crystallogr. Sect. A Found. Adv.*, 2015, **A71**, 3–8.

7 G. A. Bain and J. F. Berry, *J. Chem. Educ.*, 2008, **85**, 532–536.

8 *Gaussian 16*, Revision C.02, M. J. Frisch, G. W. Trucks, H. B. Schlegel, G. E. Scuseria, M. A. Robb, J. R. Cheeseman, G. Scalmani, V. Barone, G. A. Petersson, H. Nakatsuji, X. Li, M. Caricato, A. V. Marenich, J. Bloino, B. G. Janesko, R. Gomperts, B. Mennucci, H. P. Hratchian, J. V. Ortiz, A. F. Izmaylov, J. L. Sonnenberg, D. Williams-Young, F. Ding, F. Lipparini, F. Egidi, J. Goings, B. Peng, A. Petrone, T. Henderson, D. Ranasinghe, V. G. Zakrzewski, J. Gao, N. Rega, G. Zheng, W. Liang, M. Hada, M. Ehara, K. Toyota, R. Fukuda, J. Hasegawa, M. Ishida, T. Nakajima, Y. Honda, O. Kitao, H. Nakai, T. Vreven, K. Throssell, J. A. Montgomery, Jr., J. E. Peralta, F. Ogliaro, M. J. Bearpark, J. J. Heyd, E. N. Brothers, K. N. Kudin, V. N. Staroverov, T. A. Keith, R. Kobayashi, J. Normand, K. Raghavachari, A. P. Rendell, J. C. Burant, S. S. Iyengar, J. Tomasi, M. Cossi, J. M. Millam, M. Klene, C. Adamo, R. Cammi, J. W. Ochterski, R. L. Martin, K. Morokuma, O. Farkas, J. B. Foresman, and D. J. Fox, *Gaussian, Inc.*, Wallingford CT, 2016.

9 a) T. Yanai, D. P. Tew, N. C. Handy. *Chem. Phys. Lett.* 2004, **393**, 51–57; b) A. D. Becke. *Phys. Rev. A.* 1988, ***38***, 3098–3100; c) C. Lee, W. Yang, R. G. Parr. *Phys. Rev. B.* 1988, **37**, 785–789.

10 a) M. Dolg, H. Stoll, A. Savin, H. Preuß. *Theor. Chim. Acta.* 1989, **75**, 173–194; b) D. Andrae, U. Häußermann, M. Dolg, H. Stoll, H. Preuß. *Theor. Chim. Acta.* 1990, **77**, 123–141.

11 F. Weigend, R. Ahlrichs. *Phys. Chem. Chem. Phys.* 2005, **7**, 3297–3305.

12 a) R. Seeger, J. A. Pople. *J. Chem. Phys.* 1977, **66**, 3045–3050; b) R. Bauernschmitt, R. Ahlrichs. *J. Chem. Phys.* 1996, **104**, 9047–9052.

13 F. Neese. *WIREs Comput. Mol. Sci.* 2017, **8**, e1327; b) F. Neese, F. Wennmohs, U. Becker, C. Riplinger. *J. Chem. Phys.* 2020, **152**, 224108.

14 a) B. O. Roos in *Advances in Chemical Physics*, *Ab Initio Methods in Quantum Chemistry II*, Vol. 69 (Ed.: K. P. Lawley), Wiley, New York, 1987, pp. 399–455; b) P. Siegbahn, A. Heiberg, B. Roos, B. Levy. *Phys. Scripta*, 1980, **21**, 323–327; c) B. O. Roos, P. R. Taylor, P. E. M. Siegbahn. *Chem. Phys.*, 1980, **48**, 157–173; d) P. E. M. Siegbahn, J. Almlöf, A. Heiberg, B. Roos. *J. Chem. Phys.*, 1981, **74**, 2384–2396; e) B. O. Roos, R. Lindh, P. Å. Malmqvist, V. Veryazov, P.-O. Widmark. *Multiconfigurational Quantum Chemistry.* Wiley, Hoboken, NJ, 2016.

15 a) C. Angeli, R. Cimiraglia, S. Evangelisti, T. Leininger, J.-P. Malrieu. *J. Chem. Phys.* 2001, **114**, 10252–10264; b) C. Angeli, R. Cimiraglia, J.-P. Malrieu. *Chem. Phys. Lett.* 2001, **350**, 297–305; c) C. Angeli, R. Cimiraglia, J.-P. Malrieu. *J. Chem. Phys.* 2002, **117**, 9138–9153.

16 a) F. Neese, T. Petrenko, D. Ganyushin, G. Olbrich. *Coord. Chem. Rev.* 2007, **251**, 288–327; b) M. Atanasov, D. Aravena, E. Suturina, E. Bill, D. Maganas, F. Neese. *Coord. Chem. Rev.* 2015, **289–290**, 177–214.

17 a) F. Neese. *J. Chem. Phys.* 2005, **122**, 034107; b) A. Berning, M. Shcweizer, H.-J. Werne, P. J. Knowles, P. Palmieri. *Mol. Phys.* 2000, **98**, 1823–1833; c) B. A. Heß, C. M. Marian, U. W. Wahlgren, O. Gropen. *Chem. Phys. Lett.* 1996, **251**, 365–371.

18 a) M. Douglas, N. M. Kroll. *Ann. Phys.* 1974, **82**, 89–155; b) B. A. Heß. *Phys. Rev. A.* 1986, **33**, 3742–3748.

19 D. A. Pantazis, F. Neese. *J. Chem. Theory Comput.* 2009, **5**, 2229–2238.

20 D. A. Pantazis, X.-Y. Chen, C. R. Landis, F. Neese. *J. Chem. Theory Comput.* 2008, **4**, 908–919.